京都大学
KYOTO UNIVERSITY

KURENAI 紅
Kyoto University Research Information Repository

AGU100 ADVANCING EARTH AND SPACE SCIENCE

JGR Space Physics

RESEARCH ARTICLE

Key Points:
- Upward Poynting flux appears in the equatorward region of Region 2 FAC, which is associated with gradient of ionospheric Hall conductivity
- Morphology of Region 2 FAC depends on altitude because of significant contribution from the ionosphere
- Both magnetospheric and ionospheric processes participate in generation of Region 2 FAC and convection in the inner magnetosphere

Correspondence to:
Y. Ebihara and L. C. Lee,
ebihara@rish.kyoto-u.ac.jp;
louclee@earth.sinica.edu.tw

Energy Flow in the Region 2 Field-Aligned Current Region Under Quasi-steady Convection

Yusuke Ebihara[1], Lou-Chuang Lee[2], and Takashi Tanaka[3]

[1]Research Institute for Sustainable Humanosphere, Kyoto University, Uji, Japan, [2]Institute of Earth Sciences, Academia Sinica, Taipei, Taiwan, [3]ICSWSE, Fukuoka, Japan

Abstract We investigated energy flow in the inner magnetosphere on the basis of the results obtained by a global magnetohydrodynamic simulation. When the magnetosphere is exposed to a southward interplanetary magnetic field, the magnetosphere undergoes quasi-steady convection. Downward (earthward) Poynting flux is found in the polar cap, which is consistent with previous observations. However, Poynting flux appears to be upward (antiearthward) in the equatorward region of the auroral oval. The Region 2 field-aligned current (FAC) is embedded in the upward Poynting flux region. The upward Poynting flux is closely associated with space charge deposited by the ionospheric Hall current under inhomogeneous ionospheric conductivity. The space charge gives rise to shear flow of plasma, which is transmitted upward to the magnetosphere. The shear flow generates additional Region 2 FAC, at least, in the low-altitude magnetosphere. Spatial distribution of the Region 2 FAC appears to depend on altitude, suggesting the significant influence of the ionosphere in the Region 2 FAC region. We traced integral curves of Poynting flux (*S* curves) backward from a magnetic field line in the Region 2 FAC region and found that the *S* curves originate either in the solar wind and in the earthward-most boundary of the simulation. These simulation results suggest that the ionosphere participates in the generation of the Region 2 FAC, and the ionosphere is a mediator to feed energy to the inner magnetosphere under the quasi-steady convection.

1. Introduction

The inner magnetosphere is a key region for understanding magnetic storms. The diamagnetic current, known as a ring current, induces large-amplitude magnetic disturbances on the ground (Hoffman & Cahill, 1968). Usually, the ring current is not axisymmetric due to axisymmetric drift trajectories of particles, so that the ring current cannot be closed in the magnetosphere. The remnant of the current flows into and out of the ionosphere (Vasyliunas, 1970; Wolf, 1970). The field-aligned current (FAC) associated with the ring current is called a Region 2 FAC (Iijima & Potemra, 1976). The Region 2 FAC is suggested to have significant influence on electrodynamics in the ionosphere and the magnetosphere, such as the formation of rapid westward flow in the ionosphere (Anderson et al., 1993; Ebihara et al., 2009), overshielding (Ebihara et al., 2014; T. Kikuchi et al., 2003; Spiro & Wolf, 1984), and postmidnight enhancement of the hot ions (Ebihara & Fok, 2004; Fok et al., 2001).

The Rice Convection Model (RCM) solves motion of magnetospheric particles and obtains the Region 2 FAC from the requirement of the current closure in the magnetosphere. In the RCM, the FAC mapped to the ionosphere is used to calculate the ionospheric electric potential together with ionospheric conductance. The calculated electric field is mapped to the magnetosphere, which alters the motion of magnetospheric particles. The Region 2 FAC has also been studied by using the global magnetohydrodynamic (MHD) simulation. The magnitude of the Region 2 FAC increases with decreasing ionospheric conductance (Ridley et al., 2004), suggesting some influence of the ionospheric conductivity on the Region 2 FAC. This is consistent with the observation that the nightside Region 2 FAC in the winter hemisphere is more intense than in the summer hemisphere (Ohtani et al., 2005). The global MHD simulation also suggests that the Region 2 FAC is closely associated with a plasma flow antiparallel to the curvature vector of the magnetic field (Tanaka et al., 2016). This implies that the generation of the Region 2 FAC is related to magnetospheric processes.

FACs are closely related to the energy flow, in particular, at low altitudes (Strangeway et al., 2000). Kelley et al. (1991) made satellite observations of the field-aligned component of the quasi-DC Poynting flux and showed that the direction of the total flux is downward. Upward Poynting flux was observed in some

京都大学
KYOTO UNIVERSITY

Journal of Geophysical Research: Space Physics

10.1029/2019JA026998

京都大学学術情報リポジトリ
KURENAI 紅
Kyoto University Research Information Repository

localized regions. The contribution from the neutral wind (Thayer & Vickrey, 1992) was not clearly identified. Observations demonstrated that the downward Poynting flux is dominant at high latitudes (Gary et al., 1995; Knipp et al., 2011; Lu et al., 2018; Strangeway et al., 2000). Gary et al. (1995) showed that upward Poynting flux with small amplitudes (<0.5 mW/m^2) was identified at invariant latitudes being equal to or greater than 65°. The upward Poynting flux has also been observed at low altitudes (Kelley et al., 1991; Strangeway et al., 2005) and at high altitudes (4–8 RE; Nishimura et al., 2010). Nishimura et al. (2010) showed the upward Poynting flux during the transient events and suggested that the upward Poynting flux propagates to the magnetosphere. However, the existence of the upward Poynting flux during quasi-steady condition and the energy flow associated with the Region 2 FAC are not well understood. The purpose of this study is to clarify the role of the ionosphere in the generation of the Region 2 FAC in terms of the equation derived from Ampère's and Faraday's laws and Poynting flux on the basis of the result obtained by the global MHD simulation.

2. Simulation

We used the global MHD simulation code called REPPU (REProduce Plasma Universe; Tanaka, 2015). The REPPU code employs a grid system based on a triangle. First, we placed a sphere with a radius of 2.6 R$_E$, which is used as the inner boundary of the magnetospheric domain. The sphere is divided into 12 pentagons. Each pentagon is further divided into 5 triangles. There are 60 triangles in total in the sphere. We call this Level 1. When we further divide each triangle into 4, we obtain 240 triangles. We call this Level 2. In this particular study, we used the Level 6 grid system in which 61,440 triangles are embedded in the sphere. Three hundred twenty triangular prisms are stacked from the inner sphere outward. The outer boundary of the magnetospheric domain is located at 200 R$_E$ at midnight and 600 R$_E$ at noon. We do not solve the MHD equation in the region between 1 and 2.6 R$_E$. However, physical quantities are communicated between the inner boundary of the magnetospheric domain and the ionosphere. We calculated the ionospheric conductivity on the basis of the three sources. The first one is the conductivity associated with the ionization due to solar extreme ultraviolet, which depends on the solar zenith angle. The second one is associated with FAC, which is a proxy of discrete auroras. The third one is associated with the plasma pressure and plasma temperature, which is a proxy of diffuse auroras. On the basis of the FAC and the plasma pressure taken at the inner boundary of the magnetospheric domain, we calculated the ionospheric conductivity (both the diagonal and nondiagonal components). Readers may refer to Ebihara et al. (2014) for detailed description of the ionospheric conductivity. Solving an elliptic partial differential equation, we obtained an electric potential in the ionosphere for given FAC and ionospheric conductivity. The ionospheric electric field is mapped to the inner boundary of the magnetospheric domain (2.6 R$_E$). Thus, the magnetosphere is coupled with the ionosphere in this manner. The contribution from the neutral wind to the ionospheric electric field is excluded. In order to obtain the quasi-steady magnetosphere, we ran the simulation for 2 hr with the following parameters: solar wind velocity (V_{sw}) of 400 km/s, solar wind density (N_{sw}) of 5 cm^{-3}, interplanetary magnetic field (IMF) B_y of 0, and IMF B_z of 3.0 nT. Then, we changed IMF B_z from 3 to -5 nT at $T = 0$. The solar wind parameters were held constant at $T > 0$.

3. Results

Figure 1 shows the calculated AE (1921) index. Following the concept of the SME index (Newell & Gjerloev, 2011), we used the magnetic disturbances caused by the ionospheric Hall current at magnetic latitudes (MLATs) ranging from 50 to 90° with an interval of 1° at all magnetic local times with an interval of 0.5 hr. In total, 1,921 sampling points (=40×48+1) were used to calculate the AE index. The ionospheric Hall current was assumed to flow horizontally in a thin layer, and the magnetic disturbances were calculated by $\Delta H = I/2\mu_0$, where I is the current density above the sampling point and μ_0 is the magnetic constant. The lower and upper envelopes of the magnetic disturbance are regarded as AL and AU indices, respectively. The AL index shows an abrupt decrease at $T = 58$ min. We call this moment an expansion onset, which was identified on the basis of the criteria suggested by Newell and Gjerloev (2011). Hereinafter, we focus on the moment at $T = 48$ min, just 10 min before the expansion onset to avoid the influence of substorm expansion. This moment corresponds to the growth phase of a substorm as identified from the AL variation. The AU
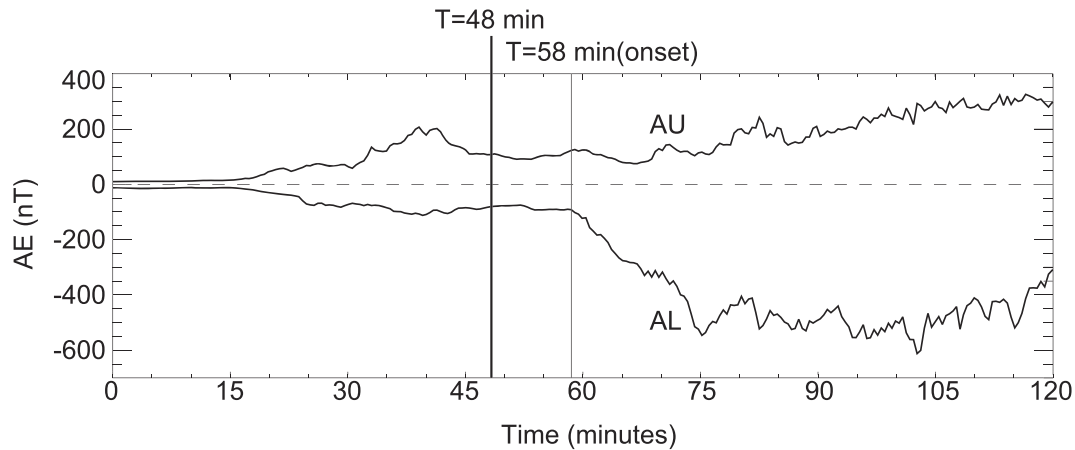
Figure 1. AE (1921) index calculated by the REProduce Plasma Universe (REPPU) code. The upper and lower lines indicate AU and AL indices, respectively.

and AL indices are almost steady around this moment, while the magnetosphere is gradually changed, such as gradual stretching of the magnetic field lines in the tail region and gradual penetration of plasma from the nightside magnetosphere to dayside.

Figure 2 shows a perspective view of the inner magnetosphere at $T = 48$ min. The view is from above the nightside tail region in the Northern Hemisphere. The plasma pressure is indicated by the greenish color in the equatorial plane. At $T = 48$ min, the plasma pressure has already been enhanced due to the enhanced magnetospheric convection. The black lines indicate the isopressure contour at 0.07 and 0.15 nPa. Simply, we regard the isopressure contour at 0.15 nPa as a proxy of the inner edge of the high-pressure region. The choice of setting the inner edge is arbitrary. However, the result is essentially unchanged regardless of the choice of the inner edge when the magnetic field line belongs to the Region 2 FACs.

Note that in the inner magnetosphere, the constant pressure contour forms a closed loop (e.g., the solid black contour line in Figure 2). In these regions, the inertial current is negligible in comparison with the diamagnetic current, and the momentum equation can be written as

$$\nabla P = \mathbf{J}_\perp \times \mathbf{B}, \tag{1}$$

where P, $\mathbf{J}_\perp$, and $\mathbf{B}$ are the plasma pressure, the perpendicular current, and the magnetic field, respectively. On the basis of the momentum equation and the current continuity, FACs are generated when the constant P contour is not aligned with the constant B contour (Hasegawa & Sato, 1989). The blue dashed lines indicate the isomagnetic field contour at 60 and 100 nT. Obviously, the isomagnetic field contour is not aligned with the isopressure contour. This is consistent with previous simulation studies (Toffoletto et al., 2003).

The eight tubes represent the magnetic field lines extending from the isopressure contour at 0.15 nPa. The tubes intersect a sphere with a radius of 3 Re. The color contour on the sphere indicates the FAC, showing that the eight magnetic field lines are connected to the Region 2 FAC region. The color on the tube indicates the parallel component of the Poynting flux, which is defined by

$$S_\parallel = \frac{\mathbf{E} \times \mathbf{B}}{\mu_0} \cdot \frac{\mathbf{B}_0}{B_0} \tag{2}$$

where $\mathbf{B}_0$ is the dipole magnetic field. It is clearly seen that the Poynting flux is upward (negative $S_\parallel$) along the field lines that belong to the Region 2 FAC. Richmond (2010) pointed out that the observed $S_\parallel$ does not always indicate the net energy transfer along a field line because of the direct contribution from the ionospheric current. This is not our case because we used the magnetic field $\mathbf{B}$ calculated only in the MHD regime and excluded the contribution from the ionospheric current.

京都大学
KYOTO UNIVERSITY

A Self-archived copy in
Kyoto University Research Information Repository
https://repository.kulib.kyoto-u.ac.jp

京都大学学術情報リポジトリ
KURENAI 紅
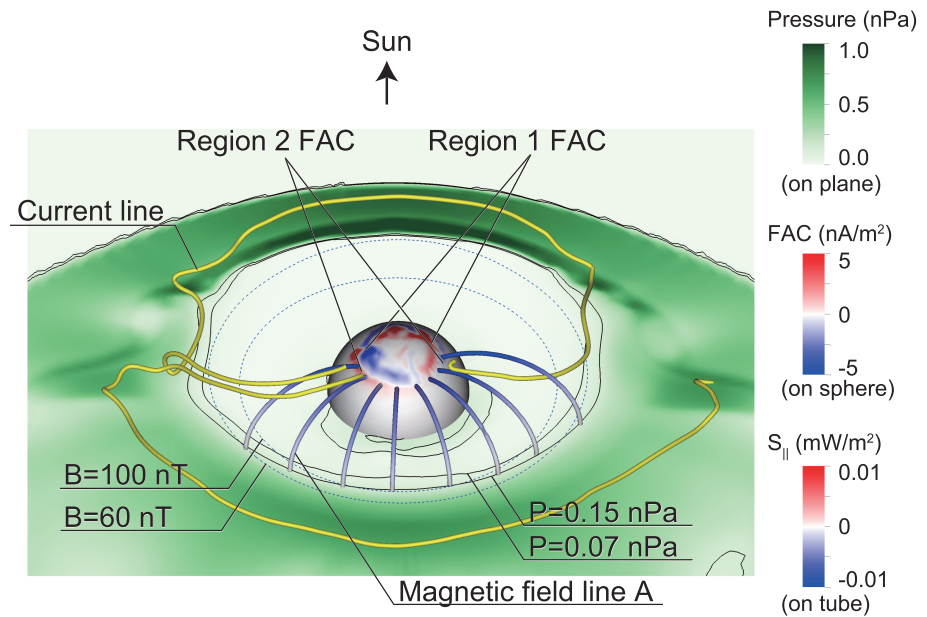Kyoto University Research Information Repository

Figure 2. Perspective view of the inner magnetosphere at $T = 48$ min (10 min before the expansion onset). The Sun is to the top. The green-white color on the equatorial plane indicates the plasma pressure. The isopressure contours at 0.07 and 0.15 nPa are indicated by the black lines. The isomagnetic field contours at 60 and 100 nT are indicated by the blue dashed lines. The color contour on the sphere with a radius of 3 R_E indicates the FACs. Eight tubes indicate the magnetic field lines with color indicated by the parallel component of the Poynting flux (negative upward). The yellow tubes indicate the current line.

As expected from equation (1), the current $\mathbf{J}_\perp$ flows along the constant P contour and forms a closed loop in the inner magnetosphere. This means that the current, flowing from the solar wind to the outer magnetosphere, cannot directly penetrate into the inner ring current region. Because of the presence of the FACs, the current line is three dimensional. Two current lines associated with the Region 2 FACs are drawn by the yellow tubes. The first one comes from the nightside magnetosphere. The morphology of the three-dimensional current line is consistent with that inferred from the global imaging ofenergetic neutral atoms (Roelof et al., 2004). The latter one comes from the dayside magnetosphere, which is consistent with that previously obtained by the MHD simulation (Ebihara et al., 2014). An important point is that the current lines are closed in the inner magnetosphere because of the requirement of the current continuity.

Figure 3 shows the parallel component of the Poynting flux $S_\parallel$ and the FAC $J_\parallel$ on a spherical surface at the geocentric distance of 3.5 R_E. Region 1 and Region 2 FACs are clearly identified. The Poynting flux is downward in the polar cap region, which is consistent with previous observations (Gary et al., 1995; Kelley et al., 1991), and global MHD simulation (Moore et al., 2014). An interesting point is that the Poynting vector appears to be upward at lower latitudes. In particular, most of the Region 2 FAC region belongs to the region where the Poynting vector is upward. We will explain the reason why the upward Poynting vector appears below.

Figure 4 is a closed-up view of the inner magnetosphere. The thin tubes indicate integral curves of the Poynting vector $\mathbf{S}$, which is called an S curve (Ebihara et al., 2019; Ebihara & Tanaka, 2017). The S curve is defined as

$$\mathbf{R}(L) = \mathbf{R}_0 + \int_{\lambda=0}^{L} \frac{\mathbf{S}(\mathbf{R}(\lambda))}{S} d\lambda, \tag{3}$$

where $\mathbf{R}$ is the position at a certain arc length L, $\mathbf{R}_0$ is the initial position, λ is an arc length from the initial position, and S is the magnitude of $\mathbf{S}$. The physical meaning of the Poynting vector comes from Poynting's theorem that states conservation of energy of the electromagnetic fields. For steady state, the Poynting
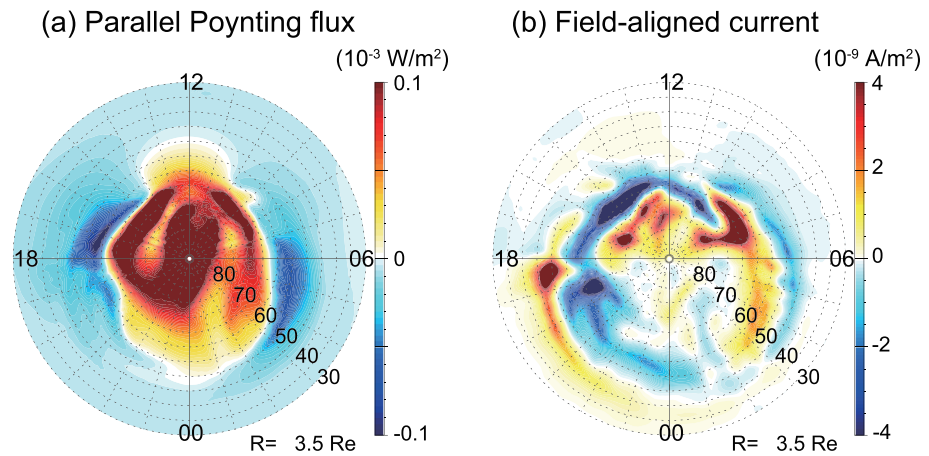
Figure 3. (a) Parallel Poynting flux $S_{||}$ (positive downward) and (b) field-aligned current $J_{||}$ (positive downward) on a sphere with a geocentric radius of 3.5 R_E at $T = 48$ min. The Sun is to the top. The outer boundary corresponds to the magnetic latitude of $30°$. The color scale is adjusted to illuminate the values in the regions of interest.

vector directs from the region where $\mathbf{J \cdot E} < 0$ (dynamo) to that where $\mathbf{J \cdot E} > 0$ (load). The relationship between the S curve and $\mathbf{J \cdot E}$ and associated energy conversion is described by Ebihara et al. (2019) and Ebihara and Tanaka (2017) in detail. Here the S curve is intended to estimate the origin of the magnetic energy consumed in the inner magnetosphere. We traced the S curve backward from two points on the magnetic field line A that belongs to the duskside Region 2 FAC. One point is located at geocentric distance of 3.4 R_E (left), and the other is at 3.2 R_E (right). As shown in the left panel, the former S curve originates in the solar wind, traveling in the magnetosphere with a spiral motion. The center of the spiral moves toward the Earth primarily due to the presence of the Region 1 FAC (Ebihara et al., 2019; Ebihara & Tanaka, 2017). The S curve eventually reached the low-altitude part of the magnetic field line A that belongs to the Region 2 FAC. In the right panel, the latter S curve is shown to originate in the earth-most boundary of the simulation. This means that the low-altitude part of the Region 2 FAC can also be associated with Poynting flux originating in the ionosphere.
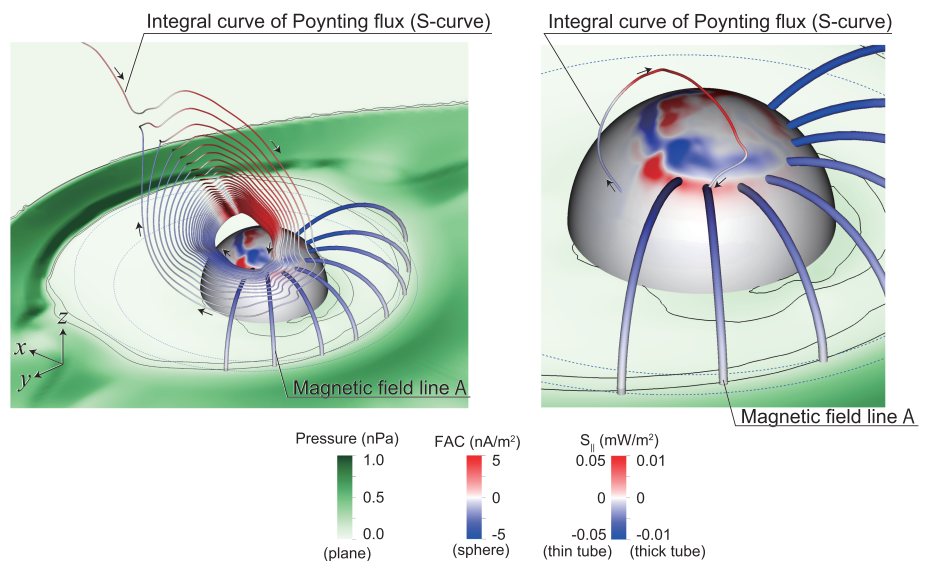

Figure 4. Same as Figure 2 except for the thin tube indicating the integral curve of the Poynting flux (S curve). The S curves are traced backward from the magnetic field line A at geocentric distances (left) 3.4 R_E and (right) 3.2 R_E. The color on the tubes indicates the parallel component of the Poynting flux $S_{||}$.
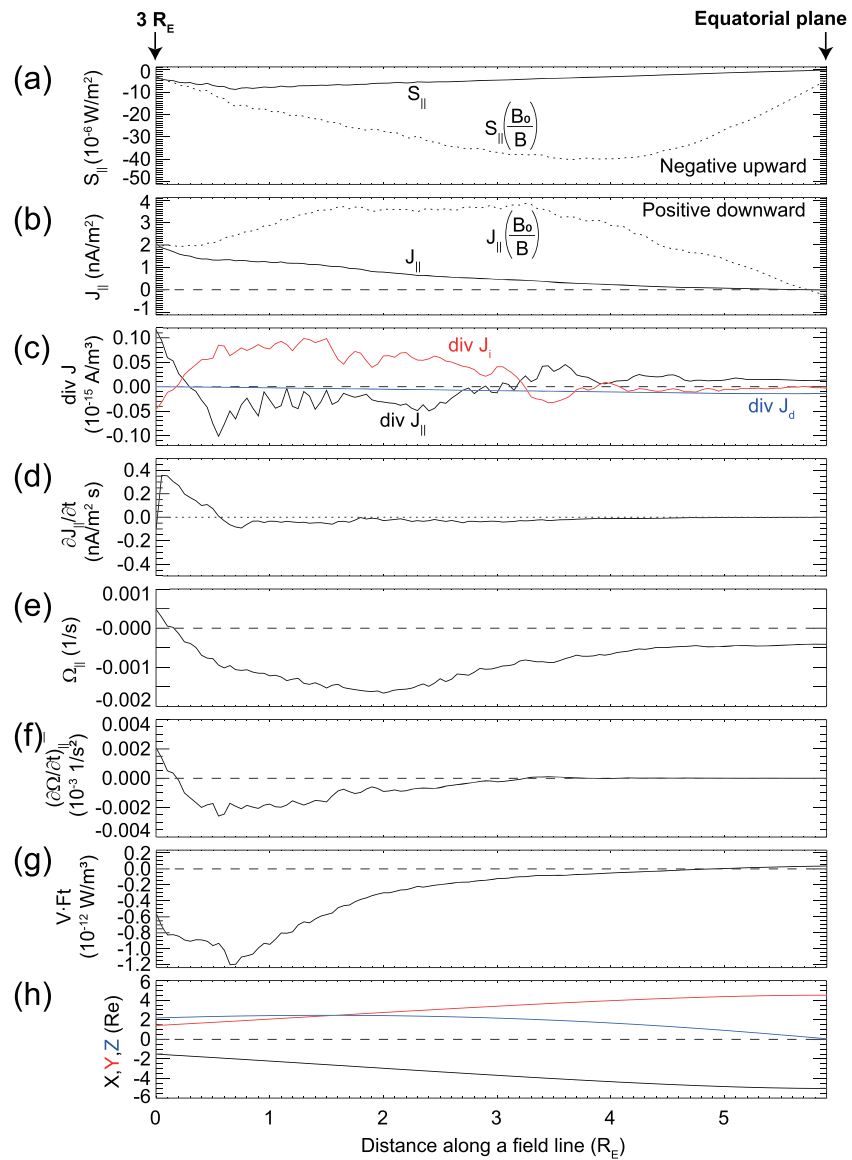
Figure 5. Quantities taken along the magnetic field line *A* (the second field line from the leftmost field one in Figures 2 and 4). (a) Parallel Poynting flux $S_{||}$; (b) field-aligned current; (c) div $\mathbf{J}_{||}$, div $\mathbf{J}_i$, and div $\mathbf{J}_d$; (d) the rate of change in the field-aligned current; (e) parallel vorticity $\Omega_{||}$; (f) parallel component of the rate of change in the vorticity; (g) $\mathbf{V}_\phi \cdot \mathbf{F}_{t,\phi}$; and (h) position of the field line. The leftmost corresponds to the geocentric distance of 3 R_E, and the rightmost corresponds to the equatorial plane. In (a) and (b), the dotted lines indicate the values multiplied by B_0/B, where B_0 is the magnetic field at distance of 0.

Figure 5. shows quantities taken along the magnetic field line *A* from the geocentric radius of 3 R_E to the equatorial plane

1. The parallel Poynting flux $S_{||}$ is upward along this field line. The value $S_{||}$ (B_0/B), where B_0 is the magnetic field at distance of zero, shows a peak at ~4 Re, which means that the parallel Poynting flux is not conserved along the field line.

2. The FAC is downward ($J_{||} > 0$) along this field line. The FAC is zero at the equatorial plane. The value $J_{||}$ (B_0/B) is not uniform along the field line, meaning that $J_{||}$ is not conserved along the field line.

3. The FAC is connected to the inertial current ($\mathbf{J}_i$) at low altitude and midaltitude, whereas it is connected to the diamagnetic current ($\mathbf{J}_d$) near the equatorial plane. $\mathbf{J}_i$ and $\mathbf{J}_d$ are given by
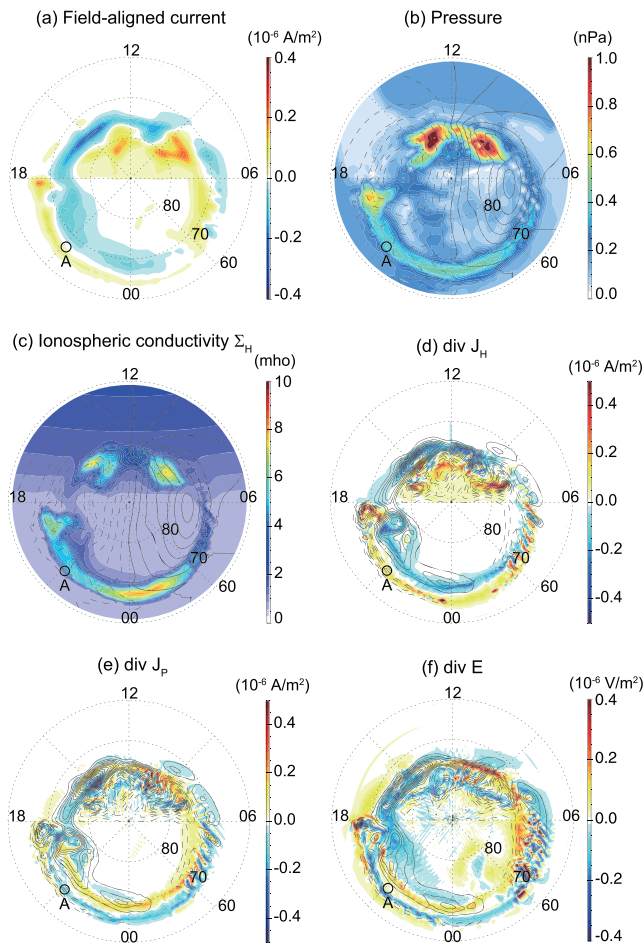
Figure 6. (a) Field-aligned current (positive downward); (b) plasma pressure mapped to the ionosphere; (c) nondiagonal component of the conductivity with contour lines indicating the ionospheric electric potential; (d) $\nabla \cdot \mathbf{J}_H$ (e) $\nabla \cdot \mathbf{J}_P$; and (f) $\nabla \cdot \mathbf{E}$ in the ionosphere at $T = 48$ min. The contour lines in (b) and (c) indicate the electric potential, and those in (d), (e), and (f) indicate the field-aligned current. The symbol A represents the footprint of the magnetic field line A (66.6 MLAT, 21.1 MLT).

$$\mathbf{J}_i = \rho \frac{\mathbf{B}}{B^2} \times \frac{d\mathbf{V}_\perp}{dt}, \tag{4}$$

and

$$\mathbf{J}_d = \frac{\mathbf{B} \times \nabla P}{B^2}, \tag{5}$$

respectively, where ρ is the mass density of plasma and P is the plasma pressure.

4. The rate of change of the FAC, which is calculated by the equation

$$\frac{\partial J_\parallel}{\partial t} \approx \frac{\nabla_\parallel (B\Omega_\parallel)}{\mu_0}, \tag{6}$$

is largely positive at low altitudes. This equation comes from Faraday's and Ampère's laws as (Ebihara & Tanaka, 2017; Song & Lysak, 2001)

$$\begin{aligned}
\frac{\partial J_\parallel}{\partial t} &= \frac{1}{\mu_0}\left[-\nabla(\nabla \cdot \mathbf{E}) + \nabla^2 \mathbf{E}\right]_\parallel = \frac{1}{\mu_0}\left[\nabla_\parallel(\nabla_\perp \cdot (\mathbf{V} \times \mathbf{B})) + \nabla_\perp^2 \mathbf{E}_\parallel\right] \\
&= \frac{1}{\mu_0}\left[\nabla_\parallel(\mathbf{B} \cdot (\nabla_\perp \times \mathbf{V}) + \mathbf{V} \cdot (\nabla_\perp \times \mathbf{B})) + \nabla_\perp^2 \mathbf{E}_\parallel\right] \\
&= \frac{1}{\mu_0}\left[\nabla_\parallel(\mathbf{B} \cdot \mathbf{\Omega}_\parallel + \mu_0 \mathbf{V} \cdot \mathbf{J}_\perp) + \nabla_\perp^2 \mathbf{E}_\parallel\right].
\end{aligned} \tag{7}$$

The second term of the last right-hand side of equation (7) is confirmed to be negligible. The third term of it is zero in the ideal MHD.

5. Interestingly, the parallel vorticity ($\Omega_\parallel = (\nabla \times \mathbf{V})_\parallel$) is positive at low altitudes ($R \sim 3$ R_E), whereas it is negative at midaltitude and high altitude. The positive gradient of parallel vorticity along the field line is found at low latitudes, which is probably associated with the generation of the downward FAC, according to equation (6).

6. The rate of change in the parallel vorticity $\Omega_\parallel$ is calculated by the following equation (Ebihara & Tanaka, 2017; Wei & Lee, 1993)

$$\mathbf{b} \cdot \frac{d\mathbf{\Omega}}{dt} = \mathbf{b} \cdot \left[\frac{1}{\rho}\nabla \times (\mathbf{J} \times \mathbf{B})\right] - \mathbf{b} \cdot \left[\frac{1}{\rho}\nabla\rho \times \frac{d\mathbf{V}}{dt}\right], \tag{8}$$

and

$$\mathbf{b} = \frac{\mathbf{B}}{B}. \tag{9}$$

The second term of the right-hand side of equation (8) is negligible because of nearly uniformity of ρ. The generation of the positive parallel vorticity at $R \sim 3$ R_E is associated with the shear flow enforced by the requirement from the ionosphere. The generation of the positive parallel vorticity gives rise to the additional downward FAC, according to equation (6).

7. $\mathbf{V}_\phi \cdot \mathbf{F}_{t,\phi}$ is largely negative at low altitudes, where $\mathbf{F}_t$ is the tension force density defined by

$$\mathbf{F}_t = \frac{B^2 (\mathbf{b} \cdot \nabla)\mathbf{b}}{\mu_0}. \tag{10}$$

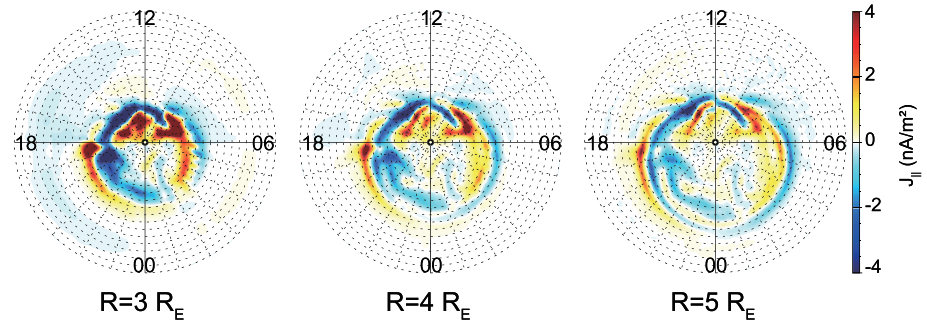Equation (10) comes from the Lorentz force as

Figure 7. Field-aligned current on the spheres at 3, 4, and 5 R_E at $T = 48$ min. The Sun is to the top. The outer circle corresponds to the magnetic latitude of 0.

$$\mathbf{J}\times\mathbf{B} = \frac{(\mathbf{B}\cdot\nabla)\mathbf{B}}{\mu_0} - \nabla\left(\frac{B^2}{2\mu_0}\right)$$
$$= \frac{B^2(\mathbf{b}\cdot\nabla)\mathbf{b}}{\mu_0} - \nabla\left(\frac{B^2}{2\mu_0}\right)_{\perp}$$

$\quad$ (11)

The first term on the right-hand side is called the tension force, and the second one is called the magnetic pressure force. The generation of FAC is related to the first term. To avoid the contribution from the curvature of the dipole (potential) magnetic field, we focus on the azimuthal component ϕ. Obviously, $\mathbf{V}_{\phi}\cdot\mathbf{F}_{t,\phi}$ is negative at low altitudes, meaning that the plasma does work against the tension force. This suggests that the azimuthal component of the flow plays a role in the generation of the FACs, in particular, at low altitudes. The generation mechanism of the azimuthal flow is described below.

Figure 6 summarizes the FACs, the nondiagonal component of the conductivity (corresponding to the Hall conductivity), $\nabla\cdot\mathbf{J}_H$ and $\nabla\cdot\mathbf{J}_P$ at the ionosphere. $\mathbf{J}_H$ and $\mathbf{J}_P$ are the height-integrated Hall current and the Pedersen current, which is given by

$$\mathbf{J}_H = \Sigma_H \frac{\mathbf{B}\times\mathbf{E}}{B},$$

$\quad$ (12)

and

$$\mathbf{J}_P = \Sigma_P\mathbf{E},$$

$\quad$ (13)

where Σ_H and Σ_P are the height-integrated Hall and Pedersen conductivities, respectively. Region 1 and 2 FACs (Iijima & Potemra, 1976) are clearly identified in Figure 6a. As shown in Figure 6b, the ionospheric conductivity Σ_H increases at 65–70 MLATs on the nightside, which resembles the auroral oval. In the REPPU code, the ionospheric conductivity is increased in accordance with the plasma pressure, temperature, and FACs. For detailed explanation, readers may refer to Ebihara et al. (2014). Figure 6c indicates $\nabla\cdot\mathbf{J}_H$. Obviously, $\nabla\cdot\mathbf{J}_H$ is nonzero in the vicinity of the auroral oval because of inhomogeneous ionospheric conductivity. This implies that FACs are connected to the Pedersen and Hall currents. From the requirement of the current continuity, the following equation must be satisfied,

$$\nabla\cdot\mathbf{J}_H + \nabla\cdot\mathbf{J}_P = -J_{\parallel}.$$

$\quad$ (14)

Figure 6d shows that $\nabla\cdot\mathbf{J}_P$ is also nonzero, meaning that space charge deposited by $\nabla\cdot\mathbf{J}_H$ cannot be fully compensated by FACs. Figure 6e shows $\nabla\cdot\mathbf{E}$, meaning the presence of space charge. Since $\nabla\cdot\mathbf{J}_P = \Sigma_P\nabla\cdot\mathbf{E} + \mathbf{E}\cdot\nabla\Sigma_P$, nonzero $\nabla\cdot\mathbf{J}_P$ is found to give rise to nonzero $\nabla\cdot\mathbf{E}$, that is, space charge. Note that $\nabla\cdot\mathbf{E} < 0$ near the equatorward boundary of the auroral oval on the nightside. Since there is no parallel electric field in the MHD simulation, the convergence of the ionospheric electric field directly corresponds to the clockwise plasma flow (or $\Omega_{\parallel} > 0$) when one views the Earth from space in the Northern Hemisphere. The clockwise plasma flow originating at low altitudes generates downward FACs, according to equation (7).

京都大学
KYOTO UNIVERSITY

A Self-archived copy in
Kyoto University Research Information Repository
https://repository.kulib.kyoto-u.ac.jp

京都大学学術情報リポジトリ
KURENAI 紅
Kyoto University Research Information Repository

Figure 7 shows the FACs at different altitudes in the magnetosphere. The morphology of the Region 2 FAC clearly depends on the altitude. At higher altitude (5 R_E), the morphology of the Region 2 FAC is determined by the magnetospheric processes, including the one previously discussed (Tanaka, 2015). At lower altitude (3 R_E), the morphology is different from that at higher altitudes and is close to the one at the ionosphere (Figure 6a). This suggests that the ionosphere participates in the generation of the Region 2 FAC.

4. Discussion and Conclusion

The global MHD simulation result shows that upward Poynting flux appears in the equatorward region of the auroral oval, including the Region 2 FAC regions. This means that the ionosphere has an active role in the Region 2 FAC regions. The active role of the ionosphere arises from space charge associated with non-zero divergence of the ionospheric Hall current. The morphology of the Region 2 FAC depends on altitude due to the active role of the ionosphere. These results should provide a word of caution about the assumption that the ionospheric FAC is a simple projection from the high-altitude magnetosphere.

It is also important to note that, as was already pointed out by Wolf (1970), the downward (upward) FAC is not always connected to the divergent (convergent) Pedersen current. When the gradient of the ionospheric conductivity is present, the downward (upward) FAC can be connected to the convergent (divergent) Pedersen current as shown in Figure 6. This should also provide a word of caution about the assumption that the downward FAC is always associated with the divergent electric field (clockwise Hall current when one views the ionosphere from space in the Northern Hemisphere).

The origin of the upward Poynting flux should be the downward Poynting flux associated with the Region 1 FAC. However, the connection between the downward and the upward Poynting fluxes is not identified in the current version of the global MHD equation because the inner boundary of the MHD domain is located at 2.6 R_E. The downward Poynting flux associated with the Region 1 FAC has been suggested to propagate horizontally in the region between the ionosphere and the ground as a waveguide mode (Kikuchi & Araki, 1979). The electric field arising in the ionosphere is expected to propagate to the inner magnetosphere (Kikuchi, 2005, 2014). The entire energy flow in the interface between the magnetosphere and the ionosphere remains unsolved. This issue will be investigated in near future.

References

Anderson, P. C., Hanson, W. B., Heelis, R. A., Craven, J. D., Baker, D. N., & Frank, L. A. (1993). A proposed production model of rapid subauroral ion drifts and their relationship to substorm evolution. *Journal of Geophysical Research*, *98*(A4), 6069. https://doi.org/10.1029/92JA01975

Ebihara, Y., & Fok, M. C. (2004). Postmidnight storm-time enhancement of tens-of-keV proton flux. *Journal of Geophysical Research*, *109*, A12209. https://doi.org/10.1029/2004JA010523

Ebihara, Y., Nishitani, N., Kikuchi, T., Ogawa, T., Hosokawa, K., Fok, M. C., & Thomsen, M. F. (2009). Dynamical property of storm time subauroral rapid flows as a manifestation of complex structures of the plasma pressure in the inner magnetosphere. *Journal of Geophysical Research*, *114*, A01306. https://doi.org/10.1029/2008JA013614

Ebihara, Y., & Tanaka, T. (2017). Energy flow exciting field-aligned current at substorm expansion onset. *Journal of Geophysical Research: Space Physics*, *122*, 12,288–12,309. https://doi.org/10.1002/2017JA024294

Ebihara, Y., Tanaka, T., & Kamiyoshikawa, N. (2019). New diagnosis for energy flow from solar wind to ionosphere during substorm: Global MHD simulation. *Journal of Geophysical Research: Space Physics*, *124*, 360–378. https://doi.org/10.1029/2018JA026177

Ebihara, Y., Tanaka, T., & Kikuchi, T. (2014). Counter equatorial electrojet and overshielding after substorm onset: Global MHD simulation study. *Journal of Geophysical Research: Space Physics*, *119*, 7281–7296. https://doi.org/10.1002/2014JA020065

Fok, M.-C., Wolf, R. A., Spiro, R. W., & Moore, T. E. (2001). Comprehensive computational model of Earth's ring current. *Journal of Geophysical Research*, *106*(A5), 8417–8424. https://doi.org/10.1029/2000JA000235

Gary, J. B., Heelis, R. A., & Thayer, J. P. (1995). Summary of field-aligned Poynting flux observations from DE 2. *Geophysical Research Letters*, *22*(14), 1861–1864. https://doi.org/10.1029/95GL00570

Hasegawa, A., & Sato, T. (1989). *Space plasma physics* (Vol. 16). Berlin, Heidelberg: Springer Berlin Heidelberg. https://doi.org/10.1007/978-3-642-74185-2

Hoffman, R. A., & Cahill, L. J. (1968). Ring current particle distributions derived from ring current magnetic field measurements. *Journal of Geophysical Research*, *73*(21), 6711–6722. https://doi.org/10.1029/JA073i021p06711

Iijima, T., & Potemra, T. A. (1976). The amplitude distribution of field-aligned currents at northern high latitudes observed by Triad. *Journal of Geophysical Research*, *81*(13), 2165. https://doi.org/10.1029/JA081i013p02165

Kelley, M. C., Knudsen, D. J., & Vickrey, J. F. (1991). Poynting flux measurements on a satellite: A diagnostic tool for space research. *Journal of Geophysical Research*, *96*(A1), 201. https://doi.org/10.1029/90JA01837

Kikuchi, T. (2005). Transmission line model for driving plasma convection in the inner magnetosphere. In R. H. W. F. T. I. Pulkkinen & N. A. Tsyganenko (Eds.), *The inner magnetosphere: Physics and modeling* (pp. 173–179). AGU.: Washington, DC. https://doi.org/10.1029/155GM20

Kikuchi, T. (2014). Transmission line model for the near-instantaneous transmission of the ionospheric electric field and currents to the equator. *Journal of Geophysical Research: Space Physics*, *119*, 1131–1156. https://doi.org/10.1002/2013JA019515

京都大学
KYOTO UNIVERSITY

A Self-archived copy in
Kyoto University Research Information Repository
https://repository.kulib.kyoto-u.ac.jp

京都大学学術情報リポジトリ
KURENAI 紅
Kyoto University Research Information Repository

Journal of Geophysical Research: Space Physics   10.1029/2019JA026998

Kikuchi, T., & Araki, T. (1979). Horizontal transmission of the polar electric field to the equator. *Journal of Atmospheric and Terrestrial Physics*, *41*(9), 927–936. https://doi.org/10.1016/0021-9169(79)90094-1

Kikuchi, T., Hashimoto, K. K., Kitamura, T. I., Tachihara, H., & Fejer, B. (2003). Equatorial counterelectrojets during substorms. *Journal of Geophysical Research*, *108*(A11), 1406. https://doi.org/10.1029/2003JA009915

Knipp, D., Eriksson, S., Kilcommons, L., Crowley, G., Lei, J., Hairston, M., & Drake, K. (2011). Extreme Poynting flux in the dayside thermosphere: Examples and statistics. *Geophysical Research Letters*, *38*, L16102. https://doi.org/10.1029/2011GL048302

Lu, Y., Deng, Y., Sheng, C., Kilcommons, L., & Knipp, D. J. (2018). Poynting flux in the dayside polar cap boundary regions from DMSP F15 satellite measurements. *Journal of Geophysical Research: Space Physics*, *123*, 6948–6956. https://doi.org/10.1029/2018JA025309

Moore, T. E., Fok, M. C., & Garcia-Sage, K. (2014). The ionospheric outflow feedback loop. *Journal of Atmospheric and Solar-Terrestrial Physics*, *115–116*, 59–66. https://doi.org/10.1016/j.jastp.2014.02.002

Newell, P. T., & Gjerloev, J. W. (2011). Evaluation of SuperMAG auroral electrojet indices as indicators of substorms and auroral power. *Journal of Geophysical Research*, *116*, A12211. https://doi.org/10.1029/2011JA016779

Nishimura, Y., Kikuchi, T., Shinbori, A., Wygant, J., Tsuji, Y., Hori, T., et al. (2010). Direct measurements of the Poynting flux associated with convection electric fields in the magnetosphere. *Journal of Geophysical Research*, *115*, A12212. https://doi.org/10.1029/2010JA015491

Ohtani, S., Ueno, G., Higuchi, T., & Kawano, H. (2005). Annual and semiannual variations of the location and intensity of large-scale field-aligned currents. *Journal of Geophysical Research*, *110*, A01216. https://doi.org/10.1029/2004JA010634

Richmond, A. D. (2010). On the ionospheric application of Poynting's theorem. *Journal of Geophysical Research*, *115*, A10311. https://doi.org/10.1029/2010JA015768

Ridley, A. J., Gombosi, T. I., & DeZeeuw, D. L. (2004). Ionospheric control of the magnetosphere: Conductance. *Annales Geophysicae*, *22*(2), 567–584. https://doi.org/10.5194/angeo-22-567-2004

Roelof, E. C., Brandt, P. C., & Mitchell, D. G. (2004). Derivation of currents and diamagnetic effects from global plasma pressure distributions obtained by IMAGE/HENA. *Advances in Space Research*, *33*(5), 747–751. https://doi.org/10.1016/S0273-1177(03)00638-0

Song, Y., & Lysak, R. L. (2001). Towards a new paradigm: From a quasi-steady description to a dynamical description of the magnetosphere. *Space Science Reviews*, *95*(1–2), 273–292. https://doi.org/10.1023/A:1005288420253

Spiro, R. W., & Wolf, R. A. (1984). Electrodynamics of convection in the inner magnetosphere. In T. A. Potemra (Ed.), *Magnetospheric Currents*, *Geophys. Monogr. Ser.* (Vol. 28, pp. 247–259). Washington, DC: AGU.

Strangeway, R. J., Elphic, R. C., Peria, W. J., & Carlson, C. W. (2000). *FAST observations of electromagnetic stresses applied to the polar ionosphere*, *Geophys. Monogr. Ser.* (pp. 21–29). Washington, DC: American Geophysical Union. https://doi.org/10.1029/GM118p0021

Strangeway, R. J., Ergun, R. E., Su, Y. J., Carlson, C. W., & Elphic, R. C. (2005). Factors controlling ionospheric outflows as observed at intermediate altitudes. *Journal of Geophysical Research*, *110*, A03221. https://doi.org/10.1029/2004JA010829

Strangeway, R. J., Russell, C. T., Carlson, C. W., McFadden, J. P., Ergun, R. E., Temerin, M., et al. (2000). Cusp field-aligned currents and ion outflows. *Journal of Geophysical Research*, *105*(A9), 21,29–21,141. https://doi.org/10.1029/2000JA900032

Tanaka, T. (2015). Substorm auroral dynamics reproduced by advanced global magnetosphere−ionosphere (M-I) coupling simulation. In *Auroral Dynamics and Space Weather* (pp. 177–190). Hoboken, NJ: John Wiley & Sons, Inc. https://doi.org/10.1002/9781118978719.ch13

Tanaka, T., Watanabe, M., den, M., Fujita, S., Ebihara, Y., Kikuchi, T., et al. (2016). Generation of field-aligned current (FAC) and convection through the formation of pressure regimes: Correction for the concept of Dungey's convection. *Journal of Geophysical Research: Space Physics*, *121*, 8695–8711. https://doi.org/10.1002/2016JA022822

Thayer, J. P., & Vickrey, J. F. (1992). On the contribution of the thermospheric neutral wind to high-latitude energetics. *Geophysical Research Letters*, *19*(3), 265–268. https://doi.org/10.1029/91GL02868

Toffoletto, F., Sazykin, S., Spiro, R., & Wolf, R. (2003). Inner magnetospheric modeling with the rice convection model. *Space Science Reviews*, *107*(1/2), 175–196. https://doi.org/10.1023/A:1025532008047

Vasyliunas, V. (1970). Mathematical models of magnetospheric convection and its coupling to the ionosphere. In B. M. McCormac (Ed.), *Particles and fields in the magnetosphere* (pp. 60–71). Dordrecht: Springer.

Wei, C. Q., & Lee, L. C. (1993). Coupling of magnetopause-boundary layer to the polar ionosphere. *Journal of Geophysical Research*, *98*(A4), 5707–5725. https://doi.org/10.1029/92JA02232

Wolf, R. A. (1970). Effects of ionospheric conductivity on convective flow of plasma in the magnetosphere. *Journal of Geophysical Research*, *75*(25), 4677. https://doi.org/10.1029/JA075i025p04677